

## Crystallographic and Electrochemical Hydrogen Storage Characteristics of $\text{La}_{0.7}\text{Ce}_{0.3}\text{Ni}_{4.2}\text{Mn}_{0.9-x}\text{Cu}_{0.3}(\text{W}_{0.42}\text{Fe}_{0.58})_x$ alloys

Mingjie Ma<sup>1</sup>, Jianchao Shi<sup>1,\*</sup>, Chen He<sup>2</sup>, Yanping Fan<sup>1</sup>, Baoqing Zhang<sup>1</sup>, Junling Sun<sup>1,\*</sup>

<sup>1</sup> School of Materials Science & Engineering, Henan Polytechnic University, Jiaozuo 454000, China

<sup>2</sup> Zhengzhou Tobacco Research Institute of China National Tobacco Corporation, Zhengzhou, Henan 450001, PR China

\*E-mail: [hpuforrest@126.com](mailto:hpuforrest@126.com); [sjl.mail@163.com](mailto:sjl.mail@163.com)

Received: 16 May 2015 / Accepted: 25 June 2015 / Published: 28 July 2015

Microstructures and electrochemical characteristics of  $\text{La}_{0.7}\text{Ce}_{0.3}\text{Ni}_{4.2}\text{Mn}_{0.9-x}\text{Cu}_{0.3}(\text{W}_{0.42}\text{Fe}_{0.58})_x$  ( $x = 0-0.20$ ) hydrogen storage alloys are systematically investigated. X-ray diffraction and backscattered electron results indicate that the pristine alloy is single  $\text{LaNi}_5$  phase, while the alloys containing  $\text{W}_{0.42}\text{Fe}_{0.58}$  consist of  $\text{LaNi}_5$  matrix phase and a trace of W segregate phase. All alloy electrodes show an excellent activation performance and can be completely activated within four charge/discharge cycles. The maximum discharge capacity of alloy electrodes first increases from 327.8 mAh/g ( $x = 0$ ) to 333.6 mAh/g ( $x = 0.10$ ), and then decreases to 328.2 mAh/g ( $x = 0.20$ ) with increasing  $x$  value. The high-rate dischargeability the alloy electrodes at the discharge current density of 1200 mA/g first increases from 60.8% ( $x = 0$ ) to 75.2% ( $x = 0.15$ ), and then decreases to 63.5% ( $x = 0.20$ ). The cycling capacity retention rate at the 100<sup>th</sup> charge/discharge cycle is decrease monotonously from 79.3 % ( $x = 0$ ) to 59.0 % ( $x = 0.20$ ) with increasing the content of  $\text{W}_{0.42}\text{Fe}_{0.58}$  alloy, which should be ascribed to the deterioration of corrosion resistance of alloy electrode in the charging/discharging cycle.

**Keywords:** Hydrogen storage alloy;  $\text{W}_{0.42}\text{Fe}_{0.58}$  alloy; Microstructure; Electrochemical property Ni/MH batteries

### 1. INTRODUCTION

Hydrogen is expected to be a promising new energy source to replace the conventional fossil for solving the shortage of fossil energy resources and the global warming in the near future. Hydrogen storage is one of many important processes in order for hydrogen to become a viable solution to the energy crisis and the environment problem [1-3]. Among different ways to store hydrogen, absorption in solid to form hydride is very attractive since it allows safe storage at pressure and temperature close

to ambient conditions [4,5]. It is the most successful for the metal hydrides to be applied as a negative electrode material in many application fields of metal hydrides. Nickel/metal hydride (Ni/MH) secondary batteries, using AB<sub>5</sub>-type hydrogen storage alloys as the negative electrode materials, have been adopted in various portable electronic devices because of their higher electrochemical performance and environment compatibility compared to the conventional Ni-Cd batteries [6,7]. Almost all of the commercial Ni/MH batteries are employing AB<sub>5</sub>-type alloys as negative electrode materials due to their good overall electrode properties [8]. However, high cost of AB<sub>5</sub>-type alloys slows down the rhythms of wide applications. Substantial efforts have been dedicated to reduce their costs by eliminating Nd and Pr [10] or substituting Co with foreign metals, such as, Mn, Fe, Cu, Si, etc [10,11]. Thereafter, the Co-free high-Mn alloys were developed and commercially produced [12]. However, the electrochemical performances, especially high-rate dischargeability, of Co-free high-Mn alloys are not yet satisfying. In our previous investigations [13,14], the commercial B<sub>0.57</sub>Fe<sub>0.43</sub> and V<sub>0.81</sub>Fe<sub>0.19</sub> alloys, rather than pure B, V or Fe, was used to substitute the Mn, which obviously decreases the cost of the alloys with the less degradation of the electrochemical hydrogen storage performances. Thus, it is feasible that the commercial alloys, rather than pure metallic elements, are used to substitute Mn in order to improving the performance-price ration of the alloys.

W is a key substitution element to improve the comprehensive electrochemical properties of hydrogen storage alloys. The appearance of W phase in rare earth-based hydrogen storage alloys can improve the discharge capacity of the alloy electrodes and the electrochemical kinetics properties [15]. The partially substituting Ni with W in La<sub>0.7</sub>Mg<sub>0.3</sub>Ni<sub>2.45-x</sub>Co<sub>0.75</sub>Mn<sub>0.1</sub>Al<sub>0.2</sub>W<sub>x</sub> ( $x=0-0.15$ ) alloys can prolong considerably the cycling stability of the hydrogen storage alloy electrodes [16]. Moreover, W was reported to be a good catalyst in improving the electrochemical kinetic properties [17]. As a result, it is essential and important to study the correlations of W on microstructures and electrochemical performances of AB<sub>5</sub>-type hydrogen storage alloys. More importantly, the price of commercial W<sub>0.42</sub>Fe<sub>0.58</sub> alloy is less than pure W, the cost of commercial W<sub>0.42</sub>Fe<sub>0.58</sub> alloy is obviously lower than that of pure W, and the melt point of W<sub>0.42</sub>Fe<sub>0.58</sub> alloy is much lower compared with pure W and the lower melt point of W<sub>0.42</sub>Fe<sub>0.58</sub> alloy facilitates the homogeneity. Fortunately, it is reported that Fe introduction in AB<sub>5</sub> alloy can remarkably improve cycling stability due to the improvement in the anti-pulverization of the alloy electrode [10,18].

Herein, on the basis of the merits of W<sub>0.42</sub>Fe<sub>0.58</sub> and the belief that the Fe and W additions may result in some noticeable modifications of electrochemical hydrogen storage performance, microstructures and electrochemical hydrogen storage characteristics of La<sub>0.7</sub>Ce<sub>0.3</sub>Ni<sub>4.2</sub>Mn<sub>0.9-x</sub>Cu<sub>0.3</sub>(W<sub>0.42</sub>Fe<sub>0.58</sub>)<sub>x</sub> ( $x = 0-0.20$ ) alloys have been investigated.

## 2. EXPERIMENTAL PROCEDURE

The investigated alloys with a nominal composition of La<sub>0.7</sub>Ce<sub>0.3</sub>Ni<sub>4.2</sub>Mn<sub>0.9-x</sub>Cu<sub>0.3</sub>(W<sub>0.42</sub>Fe<sub>0.58</sub>)<sub>x</sub> ( $x = 0-0.20$ ) alloys were prepared by arc melting in a water-cooled copper crucible of the metal elements (La, Ce, Ni, Mn Cu: 99.9% in purity and commercial W-Fe alloy contained 42 at.% W and the other were Fe and trace impurities.) under highly pure argon atmosphere. A slight excess of Mn

was used to compensate for the oxidized loss during the weigh. The cast ingots were annealed by using vacuum heat-treating furnace. Before heating, the sample cell was vacuumized until pressure is less than  $10^{-2}$  Pa and then the argon was charged into the sample cell until the pressure was 0.8 MPa. The samples were heated from room temperature to 1223 K at the rate of 10 K/min and then kept in 1223K for 6 h followed by furnace cooling.

The phase structures of the alloys was characterized by X-ray diffraction (XRD) on an X'pert PROMPD X-ray diffractometer with Cu  $K\alpha$  radiation. The alloys' power of <400 mesh size for X-ray diffraction measurement were obtained by mechanically grind the inner part of alloy ingots in the Ar atmosphere. Backscattered electron (BSE) images were obtained by using HITACHI-4800 scanning electron microscope with an energy dispersive X-ray spectrometer (EDS).

The alloy electrodes were prepared and electrochemical performances were measured by the methods in our previous literatures [13, 14]. The kinetic characteristics of the  $\text{La}_{0.7}\text{Ce}_{0.3}\text{Ni}_{4.2}\text{Mn}_{0.9-x}\text{Cu}_{0.3}(\text{W}_{0.42}\text{Fe}_{0.58})_x$  ( $x = 0-0.20$ ) alloy electrodes were performed by a PARSTAT 2273-type electrochemical workstation under room temperature in the following procedures. Linear polarization curves were obtained by scanning the electrodes from -5 to 5 mV (vs. open circuit potential) with a scan rate of 0.1 mV/s and a step height of 0.25 mV. The corrosion resistance of the alloys were characterized by the Tafel polarization, which were tested by scanning the electrodes from -250 mV to 250 mV with a scan rate of 5 mV/s and a step height of 2.5 mV. For potential-step measurement, the electrodes in fully charged state were discharged with potential steps of +500 mV potential (vs open circuit potential) and the discharge time was 3600 s.

### 3. RESULTS AND DISCUSSION

#### 3.1 Crystal structure

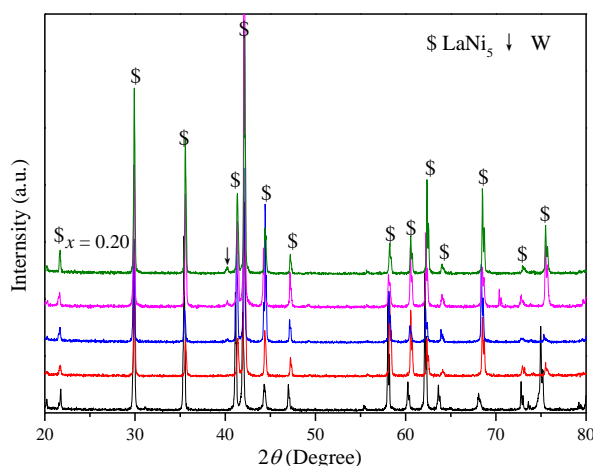


**Figure 1.** XRD patterns of  $\text{La}_{0.7}\text{Ce}_{0.3}\text{Ni}_{4.2}\text{Mn}_{0.9-x}\text{Cu}_{0.3}(\text{W}_{0.42}\text{Fe}_{0.58})_x$  alloys

Fig. 1 shows the XRD profiles of  $\text{La}_{0.7}\text{Ce}_{0.3}\text{Ni}_{4.2}\text{Mn}_{0.9-x}\text{Cu}_{0.3}(\text{W}_{0.42}\text{Fe}_{0.58})_x$  ( $x= 0-0.20$ ) hydrogen storage alloys. It can be seen that the pristine alloy is  $\text{LaNi}_5$  phase, and the alloys containing  $\text{W}_{0.42}\text{Fe}_{0.58}$  are composed of  $\text{LaNi}_5$  and W phases. BSE images and EDS results of the

La<sub>0.7</sub>Ce<sub>0.3</sub>Ni<sub>4.2</sub>Mn<sub>0.75</sub>Cu<sub>0.3</sub>(W<sub>0.42</sub>Fe<sub>0.58</sub>)<sub>0.15</sub> alloy is shown in Fig. 2. It can be seen that a mass of black grey area with sporadically distributed small quantity of white spots can be seen. EDS results of the two different area show that the continuous black gray area is LaNi<sub>5</sub> matrix phase, and the sporadic white spot is W precipitated phase.

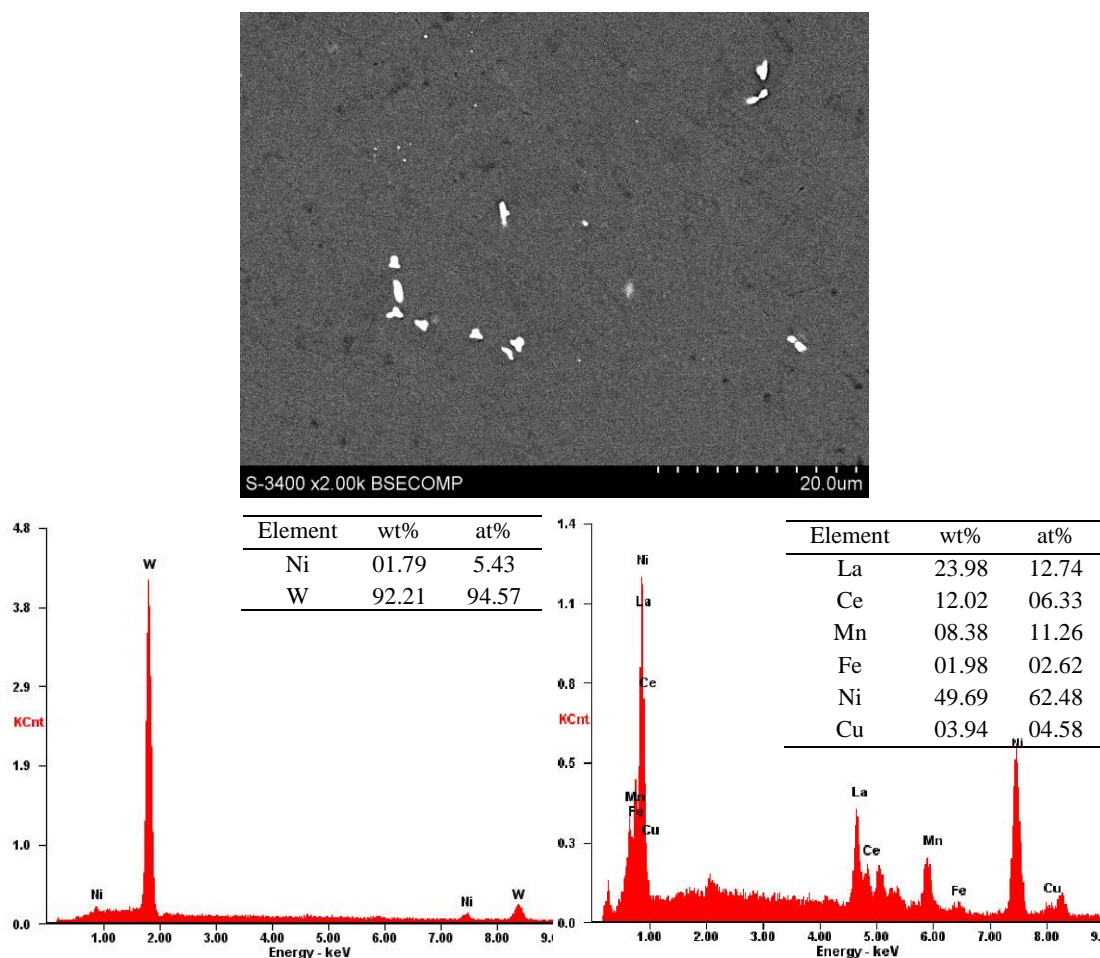


**Figure 2.** BSE and EDS results of La<sub>0.7</sub>Ce<sub>0.3</sub>Ni<sub>4.2</sub>Mn<sub>0.75</sub>Cu<sub>0.3</sub>(W<sub>0.42</sub>Fe<sub>0.58</sub>)<sub>0.15</sub> alloy (a) BSE (b) EDS of sporadic white spot (c) EDS of grey area

### 3.2 Activation and maximum discharge capability

The activation performance ( $N_a$ ) and maximum discharge capacities ( $C_{max}$ ) of all the alloy electrodes are summarized in Table 1. Results show that all alloy electrodes show an excellent activation capability. For example, all the alloy electrodes can be completely activated within four charge/discharge cycles, which also indicated that the substitution of Mn by W<sub>0.42</sub>Fe<sub>0.58</sub> alloy plays little role on the activation performance.

As shown in Table 1, the maximum discharge capacity of La<sub>0.7</sub>Ce<sub>0.3</sub>Ni<sub>4.2</sub>Mn<sub>0.9-x</sub>Cu<sub>0.3</sub>(W<sub>0.42</sub>Fe<sub>0.58</sub>)<sub>x</sub> ( $x= 0-0.20$ ) alloy electrodes first increases from 327.8 mAh/g ( $x = 0$ ) to 333.6 mAh/g ( $x = 0.10$ ), and then decreases to 328.2 mAh/g ( $x = 0.20$ ) with increasing  $x$  value. Generally, a

maximum discharge capacity of alloy electrode is related to the crystalline structure and electrochemical kinetics of the alloy. Furthermore, adding tungsten element can improve discharge capacity and speed up charge-transfer reaction on the alloy surface for AB<sub>5</sub>-type alloys [15,17]. The increase in W content with increasing  $x$  value causes the improvement in charge-transfer reaction, which is beneficial to the discharge capacity. Unfortunately, the increase in Fe content makes the surface oxide film become thicker, which degrades the charge-transfer reaction on the alloy surface. Worse still, the oxide film can decrease the number of activity sites on the alloy surface and then make the diffusion of hydrogen from the inner to the surface more difficult. Therefore, it is considered that the change of the  $C_{\max}$  of La<sub>0.7</sub>Ce<sub>0.3</sub>Ni<sub>4.2</sub>Mn<sub>0.9-x</sub>Cu<sub>0.3</sub>(W<sub>0.42</sub>Fe<sub>0.58</sub>) <sub>$x$</sub>  ( $x=0-0.20$ ) alloy electrodes should be ascribed to the combined effect of favorable and unfavorable factors.

**Table 1.** Electrochemical properties of La<sub>0.7</sub>Ce<sub>0.3</sub>Ni<sub>4.2</sub>Mn<sub>0.9-x</sub>Cu<sub>0.3</sub>(W<sub>0.42</sub>Fe<sub>0.58</sub>) <sub>$x$</sub>  alloy electrodes

$x$	$C_{\max}$ (mAh/g)	$N_a^b$	HRD <sub>1200</sub> <sup>a</sup> (%)	$S_{100}$ (%)
0	327.8	4	60.8	79.3
0.05	331.1	4	65.4	75.7
0.10	333.6	4	60.1	65.4
0.15	330.5	4	65.2	62.1
0.20	328.2	4	63.5	59.0

<sup>a</sup> The high-rate dischargeability at the discharge current density of 1200 mA/g.

<sup>b</sup> The number of cycles needed to activate the electrode.

### 3.3 High-rate dischargeability and electrochemical kinetics

The high-rate dischargeability (HRD) behavior is one of the key parameters for practical application of alloys as negative electrode materials of high-power Ni/MH batteries, which stands for overall electrochemical kinetics properties. The changing trend curve between the high-rate dischargeability and the discharge current density of La<sub>0.7</sub>Ce<sub>0.3</sub>Ni<sub>4.2</sub>Mn<sub>0.9-x</sub>Cu<sub>0.3</sub>(W<sub>0.42</sub>Fe<sub>0.58</sub>) <sub>$x$</sub>  ( $x=0-0.20$ ) alloy electrodes has present in Fig.3. Clearly, HRD of the alloy electrodes first increases with increasing  $x$  from 0 to 0.15, and then decreases when  $x$  increases to 0.20. The HRD at the discharge current density of 1200 mA/g (HRD<sub>1200</sub>) is summarized in Table 1. It can be seen that HRD<sub>1200</sub> first increases from 60.8 % ( $x=0$ ) to 75.2 % ( $x=0.15$ ), and then decreases to 63.5% ( $x=0.20$ ).

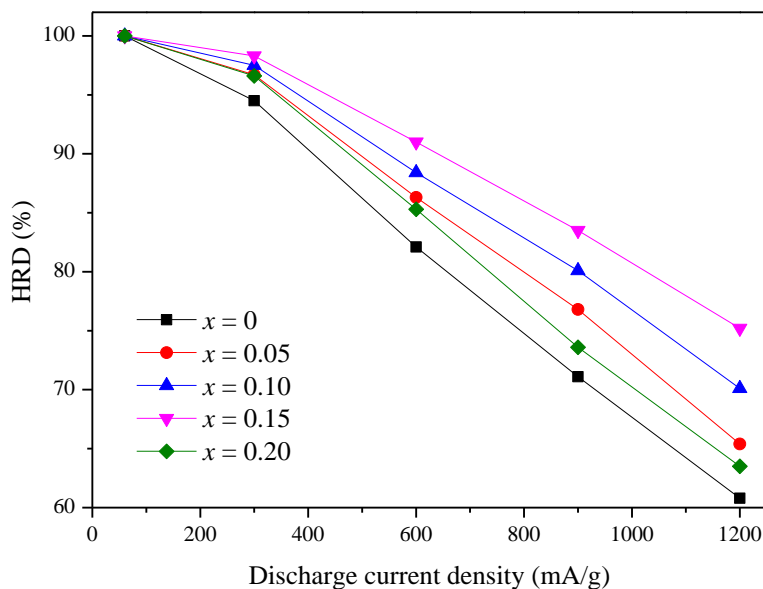


**Figure 3.** HRD of  $\text{La}_{0.7}\text{Ce}_{0.3}\text{Ni}_{4.2}\text{Mn}_{0.9-x}\text{Cu}_{0.3}(\text{W}_{0.42}\text{Fe}_{0.58})_x$  alloy electrodes

It is well-known that high-rate discharge behavior of Ni/MH battery are mainly controlled by charge-transfer between alloy the hydrogen diffusion rate from the interior of the bulk to the surface of the alloy particles [19-21], which can be evaluated by exchange current density and hydrogen diffusion coefficient, respectively [22]. In general, the exchange current density of alloy electrodes ( $I_0$ ) can be used to evaluate the charge-transfer reaction of hydrogen atom at the alloy/electrolyte interface of alloy electrodes.  $I_0$  can be calculated according to their linear polarization curves [23]:

$$I_0 = \frac{RT}{FR_p} \quad \text{Eq. (1)}$$

where  $R$ ,  $T$ ,  $F$ ,  $R_p$  are the gas constant, the absolute temperature, Faraday constant and the polarization resistance, respectively. The value of  $I_0$  of alloy electrodes was listed in Table 2. It can be seen that the maximum value (157.9 mA/g) is obtained when  $x$  value is 0.15 with increasing  $x$  value from 0 to 0.20, which indicated that a suitable addition of  $\text{W}_{0.42}\text{Fe}_{0.58}$  content is beneficial to the charge-transfer reaction of alloy electrodes. It was reported that W is a good catalyst in improving the electrochemical kinetic properties [17]. Moreover, Feng et al. [24] pointed out that W imparts desirable surface properties such as oxidation and corrosion resistance, improved porosity and electronic or ionic conductivities, which may be able to facilitate the charge-transfer process. Thus, the W precipitated phase increases with increasing  $\text{W}_{0.42}\text{Fe}_{0.58}$  content, which is beneficial to the electrocatalytic activity of the surface of alloy electrode and improves the charge-transfer reaction. Unfortunately, the increase in Fe with increasing  $x$  value will degrade the charge-transfer reaction due to increase oxide film on the alloy surface, which is detrimental to the exchange current. Therefore, it is considered that the change of  $I_0$  of  $\text{La}_{0.7}\text{Ce}_{0.3}\text{Ni}_{4.2}\text{Mn}_{0.9-x}\text{Cu}_{0.3}(\text{W}_{0.42}\text{Fe}_{0.58})_x$  ( $x=0-0.20$ ) alloy electrodes should be ascribed to the combined effect of advantage and disadvantage factors. In the study, the critical content of  $\text{W}_{0.42}\text{Fe}_{0.58}$  is  $x = 0.15$ .

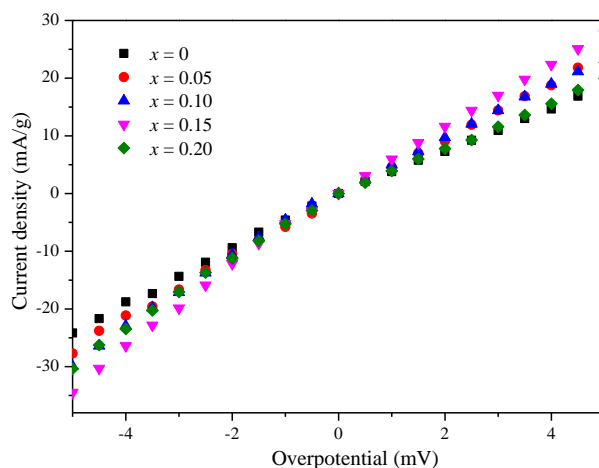


**Figure 4.** Linear polarization of  $\text{La}_{0.7}\text{Ce}_{0.3}\text{Ni}_{4.2}\text{Mn}_{0.9-x}\text{Cu}_{0.3}(\text{W}_{0.42}\text{Fe}_{0.58})_x$  alloy electrodes

**Table 2.** Electrochemical kinetic characteristics of  $\text{La}_{0.7}\text{Ce}_{0.3}\text{Ni}_{4.2}\text{Mn}_{0.9-x}\text{Cu}_{0.3}(\text{W}_{0.42}\text{Fe}_{0.58})_x$  alloy electrodes

$x$	$R_p$ ( $\text{m}\Omega \text{ g}$ )	$I_0$ ( $\text{mA/g}$ )	$D$ ( $\times 10^{-10} \text{ cm}^2/\text{s}$ )
0	234.4	109.6	3.58
0.05	196.5	130.7	3.94
0.10	183.7	139.8	5.23
0.15	162.6	157.9	5.68
0.20	202.5	126.8	3.80

The hydrogen diffusion coefficient ( $D$ ) of  $\text{LaNi}_{3.70}\text{Co}_{0.2-x}\text{Mn}_{0.30}\text{Al}_{0.15}\text{Cu}_{0.65}(\text{W}_{0.42}\text{Fe}_{0.58})_x$  ( $x=0-0.20$ ) alloy electrodes can be calculated from the slope of the linear region according to the semi-logarithmic plots of the anodic current vs. the time response, which were measured by the means of the potential-step discharge technique and has been shown Fig.5. The typical calculation method for the value of  $D$  has reported in our previous article [13]. Table 2 summarizes the  $D$  of alloy electrodes. It can be seen that the  $D$  first increases from  $3.58 \times 10^{-10}$  ( $x=0$ ) to  $5.68 \times 10^{-10} \text{ cm}^2/\text{s}$  ( $x=0.15$ ), and then decreases to  $3.80 \times 10^{-10} \text{ cm}^2/\text{s}$  ( $x=0.20$ ).

Shu et al. [25] reported the formation of the secondary phase increases the fraction of phase boundaries, which provides extra tunnels for the diffusion of hydrogen atoms. The increase of secondary phase W causes the increase in the phase boundary, which can decrease the lattice distortion and strain energy formed in the process of hydrogen absorption. On the contrary, Khaldi et al.[26] have reported that the oxidation of Fe on the alloy surface limited the hydrogen transfer from the surface to the bulk. As mentioned above, the increase of Fe content causes the increase of surface oxide film, which will degrade the hydrogen diffusion. Therefore, it is reasonable to consider that little change in

the hydrogen diffusion coefficient should be attributed to the synergetic effect of advantageous and disadvantageous factors.

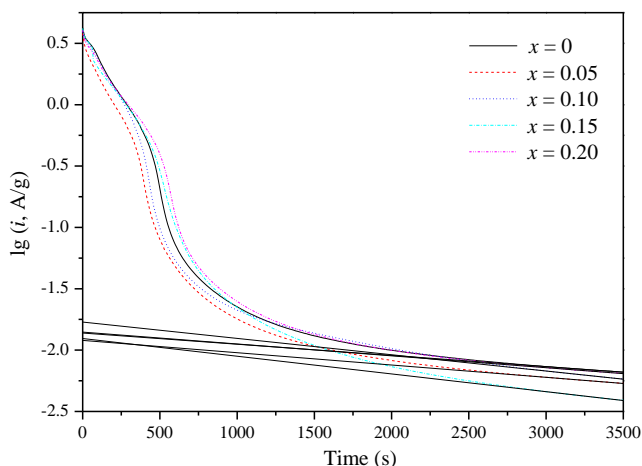


**Figure 5.** Semilogarithmic curves of anodic current vs. time of response of alloy electrodes

It was reported by Iwakura et al. [10] that, if the electrochemical reaction on the surface is the rate-determining factor, a linear dependence of the high-rate dischargeability on the exchange current density should be observed. In contrast, if the diffusion of hydrogen in the bulk is the rate-determining factor, the high-rate dischargeability should be constant, irrespective of exchange density. Fig.6 shown that the HRD at 1200 mA/g as a function of exchange current density and hydrogen diffusion coefficient for  $\text{LaNi}_{3.70}\text{Co}_{0.2-x}\text{Mn}_{0.30}\text{Al}_{0.15}\text{Cu}_{0.65}(\text{W}_{0.42}\text{Fe}_{0.58})_x$  ( $x=0-0.20$ ) alloy electrodes. It clearly that  $\text{HRD}_{1200}$  shows a linear dependence on the value of  $I_0$  and  $D$ , which indicated that the charge-transfer process at the electrode surface and hydrogen atoms diffusion process are all important factor of the electrochemical kinetics of the alloys.

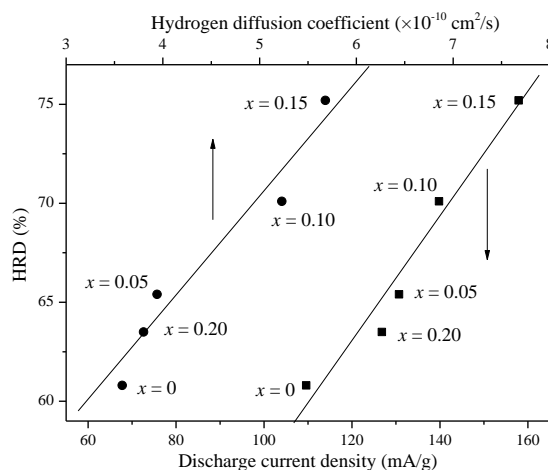


**Figure 6.** HRD at 1200 mA/g as a function of exchange current density and diffusion coefficient for alloy electrodes

### 3.4 Cycling stability

Cycling stability is an extremely important factor for the service life of hydrogen storage alloys, which directly related to the rise and fall of Ni/MH battery development. The cycle stability of the alloy electrodes at  $n^{\text{th}}$  charge/discharge cycles is characterized with the capacity retaining rates ( $S_n$ ), which can be calculated by  $S_n = C_n/C_{\text{max}} \times 100\%$  ( $C_n$  is the discharge capacity after  $n^{\text{th}}$  charge/discharge cycles,  $C_{\text{max}}$  is the maximum discharge capacity). Fig. 7 presents that the cycling stability of  $\text{La}_{0.7}\text{Ce}_{0.3}\text{Ni}_{4.2}\text{Mn}_{0.9-x}\text{Cu}_{0.3}(\text{W}_{0.42}\text{Fe}_{0.58})_x$  alloy electrodes as a function of cycle number. It can be seen that the cycling stability decreases with increasing  $x$  from 0 to 0.20. The  $S_{100}$  of the alloy electrodes are listed in Table 1. Obviously, the value of  $S_{100}$  monotonically decreases from 79.3% ( $x = 0$ ) to 59.0% ( $x = 0.20$ ). It is well known that the decay of capacity is ascribed to the pulverization and corrosion of the alloy electrode during the charging/discharging cycles [27], as well as to the decrease of the electrochemical kinetics on the alloy surface [28]. Among that, the pulverization of alloy is induced by the strain based on the lattice expansion in the charging process. The pulverized alloy creates a new surface which is oxidized when it comes into contact with the alkaline electrolyte solution. Furthermore, disintegration of alloy resulting from the pulverization leads to poor connection between particles and this induces a decreased electronic conductivity and utilization so as to decrease the cycle life. Thus, the cycle stability of the alloy mainly depends on the anti-pulverization capability of the alloy in the charging-discharging cycle. As mentioned above, the existence of the W segregate phase increases the number of phase boundary as buffer areas for the release of distortion and stress of crystal lattice in the charging/discharging process, restricted the pulverization and then improves cycling stability [29]. Moreover, it was reported by Lin et al. [30] that the increase of cell volume unit decreased the volume dilatation in the process of hydride formation, and therefore contributes to the charge-discharge life cycles. On the other hand, Fe easily oxidized due to the lower surface energy and forms coarse oxide film. The increase in Fe content not only causes the deterioration of the corrosion resistance with increasing  $x$  value and then increases the loss of the alloy, but also degrades the electrochemical kinetics on the alloy surface, which is detrimental to the discharge capacity. Worse still, the coarse oxide film on the alloy surface cannot prevents the dissolution of Mn away easily from the alloy electrode into the electrolyte.

In addition, the corrosion property of the alloy electrodes were characterized by the Tafel polarization. Fig. 8 presents the Tafel curves of  $\text{LaNi}_{3.70}\text{Co}_{0.2-x}\text{Mn}_{0.30}\text{Al}_{0.15}\text{Cu}_{0.65}(\text{W}_{0.42}\text{Fe}_{0.58})_x$  alloy electrodes. Clearly, the corrosion potential of alloy electrodes becomes more negative while the corrosion current increases with increasing  $x$  value, which is indicated that the corrosion resistance of alloy electrodes decreases with increasing the content of  $\text{W}_{0.42}\text{Fe}_{0.58}$  alloy. Therefore, it is confirmed that the decrease in corrosion resistance of alloy electrodes is the critical reasons for the degradation of cycling stability.

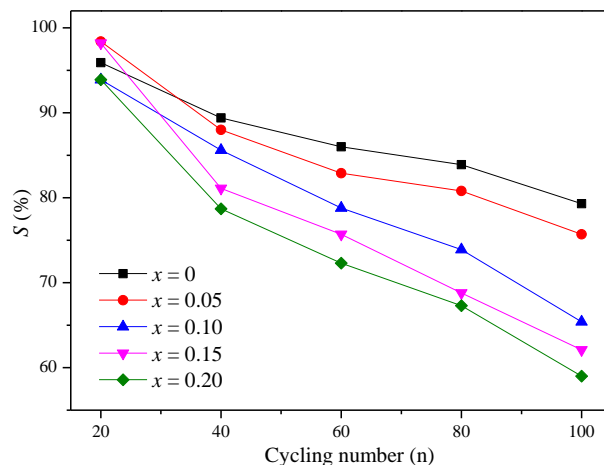


**Figure 7.** Cycling stability of  $\text{La}_{0.7}\text{Ce}_{0.3}\text{Ni}_{4.2}\text{Mn}_{0.9-x}\text{Cu}_{0.3}(\text{W}_{0.42}\text{Fe}_{0.58})_x$  alloy electrodes

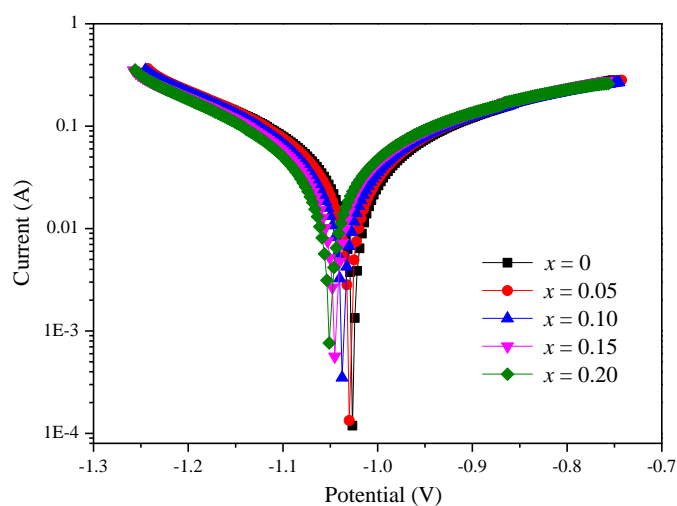


**Figure 8.** Tafel curves of  $\text{La}_{0.7}\text{Ce}_{0.3}\text{Ni}_{4.2}\text{Mn}_{0.9-x}\text{Cu}_{0.3}(\text{W}_{0.42}\text{Fe}_{0.58})_x$  alloy electrodes

#### 4. CONCLUSIONS

In this paper, microstructures and electrochemical characteristics of  $\text{La}_{0.7}\text{Ce}_{0.3}\text{Ni}_{4.2}\text{Mn}_{0.9-x}\text{Cu}_{0.3}(\text{W}_{0.42}\text{Fe}_{0.58})_x$  ( $x = 0-0.20$ ) hydrogen storage alloys are systematically investigated. The following conclusions can be drawn:

1. Analysis of X-ray diffraction profiles and backscattered electron results shows that the pristine alloy is single  $\text{LaNi}_5$  phase with a hexagonal  $\text{CaCu}_5$ -type structure, while the alloys containing  $\text{W}_{0.42}\text{Fe}_{0.58}$  consist of  $\text{LaNi}_5$  matrix phase and a trace of W segregate phase.

2. All alloy electrodes show an excellent activation performance and can be completely activated within four charge/discharge cycles, which also indicated that the substitution of Mn by  $\text{W}_{0.42}\text{Fe}_{0.58}$  alloy plays little role on the activation performance. The maximum discharge capacity of alloy electrodes first increases from 327.8 mAh/g ( $x = 0$ ) to 333.6 mAh/g ( $x = 0.10$ ), and then decreases to 328.2 mAh/g ( $x = 0.20$ ) with increasing  $x$  value.

3. The high-rate dischargeability the alloy electrodes at the discharge current density of 1200 mA/g first increases from 60.8% ( $x = 0$ ) to 75.2% ( $x = 0.15$ ), and then decreases to 63.5% ( $x = 0.20$ ). This is consistent with the variation tendency of exchange current density and hydrogen diffusion coefficient.

4. The cycling capacity retention rate at the 100<sup>th</sup> charge/discharge cycle is decrease monotonously from 79.3 % ( $x = 0$ ) to 59.0 % ( $x = 0.20$ ) with increasing the content of  $W_{0.42}Fe_{0.58}$  alloy, which should be ascribed to the deterioration of corrosion resistance of alloy electrode in the charging/discharging cycle.

## Reference

1. L.Z. Ouyang, C.H. Peng and M. Zhu, *Int. J. Hydrogen Energy*, 32 (2007) 3929-3935.
2. Z.J. Cao, L.Z. Ouyang, H. Wang, D.L. Sun, Q.A. Zhang and M. Zhu, *J. Alloys Compd.*, 608 (2014) 14.
3. J.B. Tan, X.Q. Zeng, J.X. Zou, X.M. Wu, W.J. Ding, *Trans. Nonferrous Met. Soc. China*, 23 (2013) 2307.
4. Y. Fukumoto, M. Miyamoto, M. Matsuoka and C. Iwakura, *Electrochim. Acta*, 40 (1995) 845.
5. L.Z. Ouyang, J.M. Huang, H. Wang, Q.A. Zhang, D.L. Sun and M. Zhu, *Int. J. Hydrogen Energy*, 38 (2013) 2973.
6. H.G. Pan, J.X. Ma, C.S. Wang, C.P. Chen, Q.D. Wang, *Electrochim. Acta*, 44 (1999) 3977.
7. M. Tliha, H. Mathlouthi, J. Lamoumi, A. Percheron-Guegan, *J. Alloys Compd.*, 436 (2007) 221.
8. X.D. Wei, P. Zhang, H. Dong, Y.N. Liu, J.W. Zhu and G. Yu, *J. Alloys Compd.*, 458 (2008) 583.
9. L.Z. Ouyang, Z.J. Cao, L.L. Li, H. Wang, J.W. Liu, D. Min, Y.W. Chen, F.M. Xiao, R.H. Tang and M. Zhu, *Int. J. Hydrogen Energy*, 39 (2014) 12765.
10. C. Iwakura, K. Ohkawa, H. Senoh and H. Inoue, *Electrochim. Acta*, 46 (2001) 4383.
11. B. Zhang, W.Y. Wu, B. Xue and G.F. Tu, *J. Alloys Compd.*, 538 (2012) 189.
12. K. Komori, O. Yamamoto, Y. Toyoguchi, K. Suzuki, S. Yamaguchi, A. Tanaka, M. Ikoma, US5512385 (1996)
13. X. Peng, B. Liu, Y. Fan, X. Zhu, Q. Peng and Z. Zhang, *J. Power Sources*, 240 (2013) 178.
14. X. Peng, B. Liu, Y. Fan, L. Ji, B. Zhang and Z. Zhang, *Electrochim. Acta*, 93 (2013) 207.
15. J. Liu, W.H. Wang, S.H. Ye, X.P. Gao, H.T. Yuan, D.Y. Song and Y.S. Zhang, *J. Alloys Compd.*, 285 (1999) 263.
16. H.G. Pan, X.F. Wu, M.X. Gao, N. Chen, Y.J. Yue and Y.Q. Lei, *Int. J. Hydrogen Energy*, 31 (2006) 517.
17. H. Ye and H. Zhang, *Adv. Eng. Mater.*, 3 (2001) 481.
18. B. Liao, Y.Q. Lei, L.X. Chen, G.L. Lu, H.G. Pan and Q.D. Wang, *J. Alloys Compd.*, 376 (2004) 186.
19. Y. Li, S. Han, J. Li, X. Zhu and L. Hu. *J. Alloys Compd.*, 458 (2008) 357.
20. C. Iwakura, T. Oura, H. Inoue and M. Matsuoka, *Electrochim Acta*, 41 (1996) 117.
21. Y. Sakamoto, K. Kuruma and Y. Naritomi, *Berichte der Bunsengesellschaft für physikalische Chemie.*, 96 (1992) 1813.
22. F.L. Zhang, Y.C. Luo, J.P. Chen, R.X. Yan and J.H. Chen, *J. Alloys Compd.*, 430 (2007) 302.
23. P.H.L. Notten and P. Hokkeling, *J. Electrochem. Soc.*, 138 (1991) 1877
24. F. Feng, M. Geng, D.O. Northwood, *Int. J. Hydrogen Energy*, 26 (2001) 725.
25. K.Y. Shu, S.K. Zhang, Y.Q. Lei, G.L. Lü and Q.D. Wang, *Int. J. Hydrogen Energy*, 28 (2003) 1101.

26. C. Khaldi, H. Mathlouthi, J. Lamloumi and A. Percheron-Guegan, *J. Alloys Compd.*, 360 (2003) 266.
27. D. Chartouni, F. Meli, A. Züttel, K. Gross and L. Schlapbach, *J. Alloys Compd.*, 241 (1996) 160.
28. B.Z. Liu, G.X. Fan, Y.C. Wang, G.F. Mi, Y.M. Wu and L.M. Wang, *Int. J. Hydrogen Energy*, 33 (2008) 5801.
29. P. Li, X.L. Wang, Y.H. Zhang, R. Li, J.M. Wu and X.H. Qu, *J. Alloys Compd.*, 353 (2003) 278.
30. Q. Lin, S. Zhao, D.J. Zhu, B. Song and Z. Mei, *J Alloys Compd.*, 351 (2003) 91.

© 2015 The Authors. Published by ESG ([www.electrochemsci.org](http://www.electrochemsci.org)). This article is an open access article distributed under the terms and conditions of the Creative Commons Attribution license (<http://creativecommons.org/licenses/by/4.0/>).